Appl Nanosci (2013) 3:295–302
DOI 10.1007/s13204-012-0147-z

ORIGINAL ARTICLE

Change in the morphology of ZnO nanoparticles upon changing the reactant concentration

Mohammad Ali Moghri Moazzen · Seyed Majid Borghei · Farshad Taleshi

Received: 3 January 2012 / Accepted: 9 July 2012 / Published online: 28 July 2012

Abstract ZnO plays an important role in many technological aspects of semiconductors. Because of its interesting properties, it has attracted a great deal of attention for a wide range of applications. In this work, the direct precipitation method was employed for the synthesis of ZnO nanoparticles to study the role of different concentration ratios of reactants on the crystal structure, size, and morphology of the prepared ZnO nanoparticles. The reactant raw materials used in this experiment were zinc acetate dihydrate as a zinc source and NaOH. ZnO nanoparticles were synthesized by calcination of the ZnO precursor precipitates at 250 °C for 3 h. These calcinated ZnO nanoparticles and their properties were characterized using X-ray diffraction, a scanning electron microscope equipped with an energy dispersive X-ray spectrometer, and transmission electron microscopy. We present the experiment conditions, including result on the different reactant concentration ratios, which affect the control of the size and morphology of the ZnO nanoparticles. The mean size of the ZnO nanoparticles was 18 nm.

Keywords Synthesis of ZnO nanoparticles · Direct precipitation method · Different concentration ratios · Characterization · Particle size distribution

M. A. Moghri Moazzen
Young Researchers Club, Karaj Branch,
Islamic Azad University, Karaj, Iran

S. M. Borghei (✉)
Department of Physics, Karaj Branch,
Islamic Azad University, Karaj, Iran
e-mail: majid.borghei@kiau.ac.ir

F. Taleshi
Department of Applied Science, Qaemshahr Branch,
Islamic Azad University, Qaemshahr, Iran

Introduction

Among the more well-known semiconductor materials, ZnO is a II–VI semiconducting ceramic material that possesses a wide band gap of $E_g = 3.37$ eV and a large exciton binding energy of 60 meV at room temperature (Huang et al. 2001). The importance of this material is reflected in its excellent chemical, mechanical, electrical, optical and optoelectrical properties. For example, it provides both good electrical conductivity (Nakahara et al. 2001) and high transmittance. ZnO has great applicability in the preparation of solar cells (Wang et al. 2001), gas sensors (Lin et al. 1998; Xu et al. 2000), transparent electrodes (Sahu et al. 2007), piezoelectric materials (Wang and Song 2006), and varistors (Koch et al. 1995). However, these are simply a few examples that illustrate its importance. For further indication of its significance, the reader directed to "Appendix".

Nanoparticles are also one of the key elements in nanotechnology. Therefore, in this study we attempt to evaluate the role of different concentration ratios of reactants on ZnO nanoparticles synthesized via the direct precipitation method (DPM). There are also some other parameters that are important in preparation of ZnO nanoparticles by this method and which impact the size and distribution of the nanoparticles, such as the reaction temperature or stirring. Understanding these parameters is important because the properties of these particles depend closely on their size and morphology (Dai et al. 2003).

Over the past twenty years, ZnO nanostructures with various morphologies have been synthesized using a large variety of methods. Such systems provide a rich family of morphologies in comparison to other materials and, as a review of this wide range of nanostructures, we have listed some of these morphologies in "Appendix" so as to present

a pertinent background on the works carried out on this important semiconductor material.

Different synthesis methods for the preparation of ZnO nanostructures have been employed in the literature including sol–gel (Tokumoto et al. 2003; Hohenberger et al. 1992), micro-emulsion (Singhal et al. 1997), mechano-chemical processing (Tsuzuki and McCormick 2001), vapour phase transport (Zhang et al. 2005), chemical vapour deposition (Wu and Liu 2002), hydrothermal processing (Zhang et al. 2004; Liu and Zeng 2003), spray pyrolysis and drying (Park and Kang 1997; Okuyama and Lenggoro 2003), supercritical-water processing (Viswanthan et al. 2003), thermal decomposition of organic precursor (Rataboul et al. 2002), radio frequency plasma synthesis (Sato et al. 2003), self-assembly (Koh et al. 2004), sono-chemical or microwave-assisted synthesis (Hu et al. 2004), homogenous precipitation (Kim et al. 2005) and direct precipitation (Wang and Gao 2003).

In the present study, as mentioned vide supra, ZnO nanoparticles were prepared by precipitation from zinc acetate dihydrate and sodium hydroxide. This method exhibits several advantages over the others listed, such as low cost, large-scale production, low-temperature, and the reduced need for equipment or catalyst assistance. ZnO nanoparticles were obtained and their sizes, morphologies, and structures characterized using X-ray diffraction (XRD), scanning electron microscopy (SEM), energy-dispersive X-ray (EDX) spectroscopy and transmission electron microscopy (TEM). The ratio of the concentration of zinc acetate dihydrate:sodium hydroxide precursor was varied from 1:1 to 1:4 and the size and morphology of the particles were found to depend strongly on this ratio.

The paper is organized as follows. Previously published works on the synthesis of ZnO nanoparticles were briefly reviewed above. In the section that immediately follows, the main conditions and key parameters of our experiments by the DPM, including the synthesis process, are presented using a schematic diagram. Results obtained by the change in the concentration ratio of the reactant raw materials used in the experiment, and its effect on controlling the size and morphology of the ZnO nanoparticles, are then discussed and show that these properties are size-dependent. Finally, we provide a summary of our findings and present some conclusions.

Material and experimental procedure

Reactant raw materials

Zinc acetate dihydrate (as a Zinc source), sodium hydroxide, ethanol, and distilled deionized water were used in the experiments described herein. Zinc acetate dihydrate and sodium hydroxide were used as the precursors for the formation of ZnO particles.

Synthesis of ZnO nanoparticles

The schematic diagram illustrating the synthesis procedures (DPM) for ZnO particles is presented in Fig. 1.

First, zinc acetate dihydrate (Merck, 99 %) and sodium hydroxide (Merck, 99 %) were each dissolved in distilled deionized water to form liquid media of the desired concentrations. The zinc acetate dihydrate solution was slowly added drop-wise to the sodium hydroxide solution under vigorous stirring at room temperature, forming a transparent white solution. In this way, different concentration ratios of aqueous solutions of zinc acetate dihydrate to sodium hydroxide were prepared. The ratio of the concentrations was varied from 1:1 to 1:4 (zinc acetate dihydrate:sodium hydroxide). These solutions were slowly reacted to produce ZnO particle precipitates. In the next step, the precipitates obtained upon the reaction between the zinc acetate dihydrate and sodium hydroxide solutions were collected by filtration and rinsed three times with distilled deionized water and ethanol. Following this, the washed precipitates were dried in an electric oven at 100 °C for 5 h until ZnO precursors formed. At the final

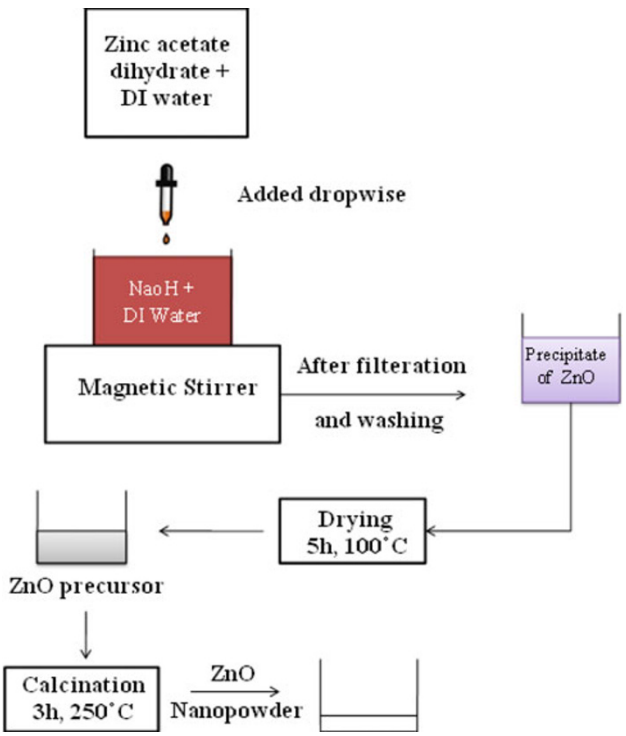

Fig. 1 Schematic diagram showing the preparation of ZnO nanoparticles

step, the precursors were calcinated at 250 °C for 3 h to obtain ZnO nanopowder.

Results and discussion

X-ray diffraction

Analysis of the crystal structures of the ZnO nanoparticles prepared by the DPM was performed with an X-ray diffractometer (MMA, GBC, Australia) using Cu Kα radiation. The diffractograms, which are provided in Fig. 2, we recorded in the 2θ range of 20° to 80° with a step size of 0.05° and scan time of 1 s per step.

The four distinct results (a–d) correspond to the different precipitator concentration ratios (zinc acetate dihydrate: sodium hydroxide) of 1:1, 1:2, 1:3, and 1:4, respectively. The prominent peaks labeled on the figure and which were observed at angles of 31.6°, 34.2°, 36.1°, 47.3°, 56.3°, 62.7°, 66.2°, 67.5° and 68.8° belong to the (100), (002), (101), (102), (110), (103), (200), (112), and (201) planes, respectively. These peaks show very good agreement with the reported values of the Joint Committee on Powder Diffraction Standards data (JCPDS 36-1451) and confirm the formation of hexagonal wurtzite zinc oxide (Lepkova et al. 2007; Bhat 2008). No peaks that may correspond to impurities were detected, thus implying that a relatively high purity of ZnO nanoparticles was obtained. EDX spectroscopy was then used to provide elemental analysis and study the compositions of the particles, with the obtained spectrum displayed in Fig. 3.

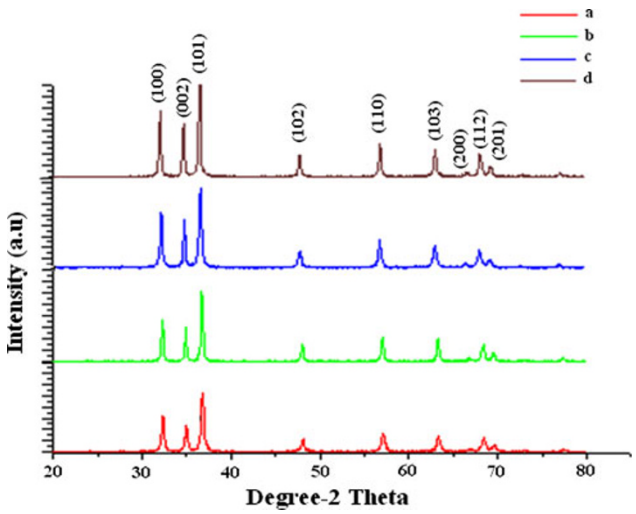

Fig. 2 XRD patterns of ZnO nanopowder synthesized under different ratio of precursor concentration **a** 1:1, **b** 1:2, **c** 1:3, **d** 1:4

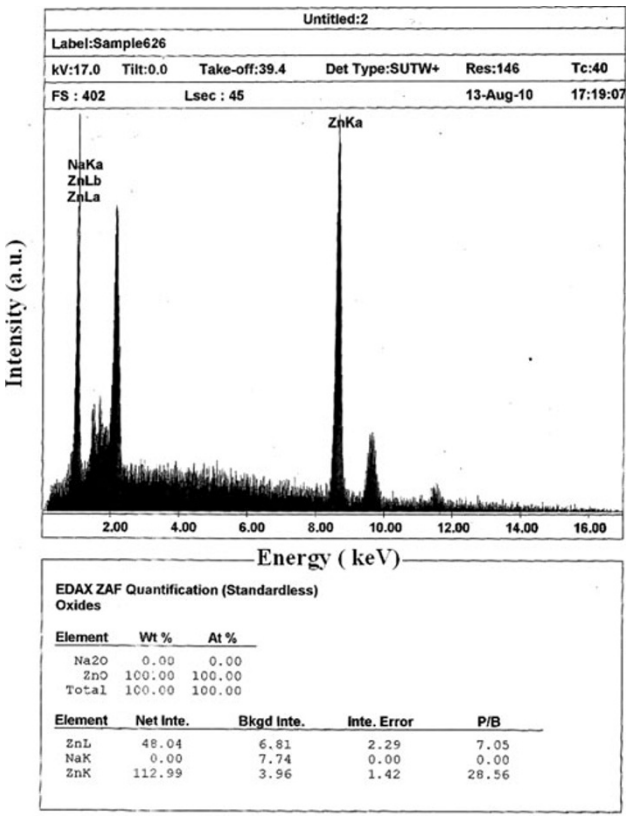

Fig. 3 EDX spectrum of the ZnO particles

Figure 3 clearly shows that only Zn and O atoms are present, as evidenced by the determined spectrum. In other words, the product is composed 100 % (Wt and At) of ZnO. We cannot observe the O peaks that must be present from the ZnO because this analysis was carried out using an instrument that cannot depict elements lighter than Na. Figures 2 and 3 both confirm the formation of pure ZnO particles.

The average crystallite size of the obtained particles was measured from the broadening of the diffraction peaks and application of the Scherrer formula (West 1985).

$$D = (0.89\lambda)/(\beta \cos\ \theta) \quad (1)$$

Therein, λ is the wavelength of the Cu kα radiation (1.54 Å), β is the full width at half maximum of the peak, and θ is the Bragg's angle obtained from the 2θ value corresponding to the maximum intensity peak in XRD pattern. The measured values varied between 20 and 36 nm for samples a–d, as described in Table 1.

As the reactant raw material concentration ratios increases from 1:1 to 1:4, the intensity of the reflections peaks increases, as can be seen from Fig. 2. Therefore, of the samples studied, ZnO nanopowder at a concentration

Table 1 Crystallite sizes according to the major diffraction peaks observed in Fig. 2

Samples	Concentration ratio	FWHM (°)	Particle sizes (nm)
a	1:1	0.44	20
b	1:2	0.30	27
c	1:3	0.27	30
d	1:4	0.23	36

ratio of 1:4 has the most intense peaks and largest crystallite size of 36 nm.

Scanning electron microscopy

The morphologies of the nanoparticles were analyzed using a scanning electron microscope (Philips) equipped with an energy-dispersive X-ray spectrometer. The EDX spectroscopy results were discussed in the previous section.

Figures 4a–d show SEM micrographs of the ZnO particles prepared at different ratios of reactant concentration.

These images clearly show remarkably different morphologies for these ZnO particles. As can be seen from Fig. 4a, at a concentration of 1:1 the nanoparticles are spherical, whereas at a concentration of 1:2, they are cauliflower-like (Fig. 4b). By further increasing the concentration ratio, the clusters become irregularly shaped and non-uniform. As the concentration ratio was gradually increased, the average size of the nanoparticles increased from 18 to 36 nm. From the aforementioned results, it is therefore concluded that the sizes and morphologies of as-prepared ZnO powders depends markedly on the concentration ratio of the reactants. Furthermore, as the nanoparticles become smaller, the surface-to-volume ratio

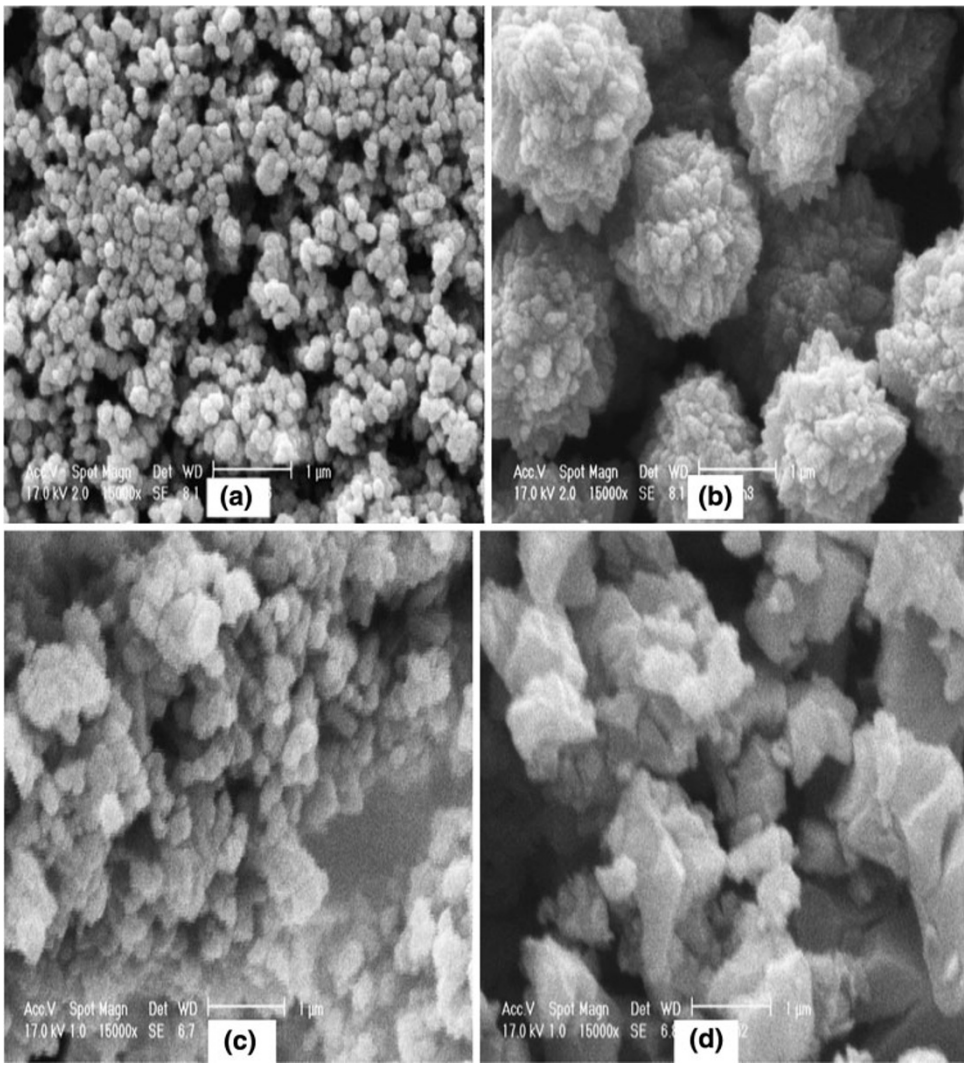

Fig. 4 SEM images of ZnO nanopowder synthesized under different ratios of precursor concentration **a** 1:1, **b** 1:2, **c** 1:3, **d** 1:4

or nanoparticles aspect ratio increases and their chemical reactivity increases.

Transmission electron microscopy

The synthesized ZnO nanoparticles were further characterized using transmission electron microscopy (TEM) (CM10, Philips). Figure 5, which shows a typical TEM image obtained for the sample a, gives further insight into some noteworthy details of the formed particles.

As can be seen from Fig. 5, the ZnO nanoparticles are approximately spherical in shape, confirming the findings obtained by SEM (see Fig. 4a). A histogram (Fig. 6) illustrates the distribution in nanoparticle size; with this figure indicating that a normal distribution of nanoparticles was obtained, centered at a diameter of 15–20 nm. Thus, our samples have a high surface area, making them appropriate for catalytic applications. The higher surface area is attributed to the formation of smaller particles. Photocatalytic activity of ZnO nanoparticles depends on the surface area. Due to the unique properties originating from their high surface area, ZnO nanoparticles and more generally, semiconductor nanoparticles are subjected to much research attentions. Also, synthesis method provides control over the surface area.

Discrepancies in the estimation of nanoparticle size by the different techniques used in this work can be understood. We know that under optimal conditions the precision of the Debye–Scherrer in measuring crystallite size is in the order of ±10 % (Cullity 1978; Azaroff 1968). Therefore, the actual average size of the nanoparticles in this work, as determined by TEM, is 18 nm. However, the nanoparticle size estimated by XRD, which identifies the underlying lattice planes,

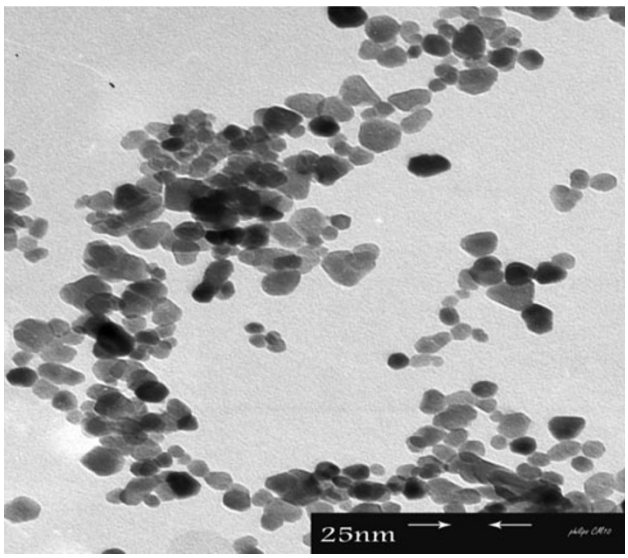

Fig. 5 TEM image of ZnO nanoparticles

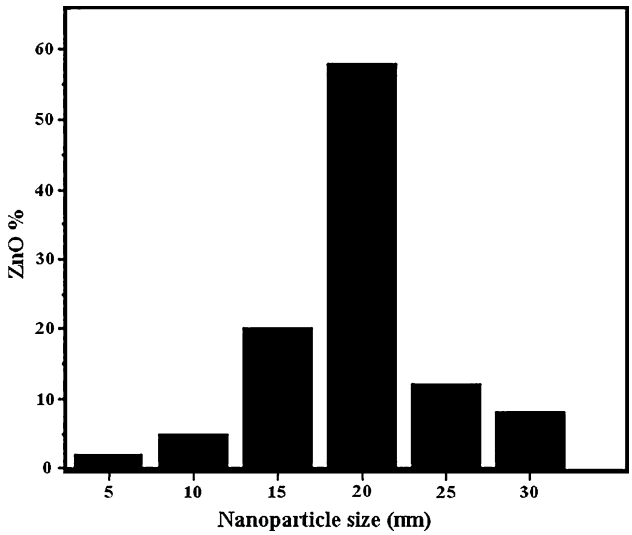

Fig. 6 A histogram representing distribution of ZnO nanoparticles prepared at 1:1 concentration ratio

is 20 nm. Therefore, this value for nanoparticle size is within an acceptable precision limit to the TEM result.

Conclusion

In this work, ZnO nanoparticles were synthesized using the direct precipitation method at room temperature. The advantages of this method are that a large quantity of ZnO nanoparticles can be synthesized with high purity and a low cost of production. The role of different concentration ratios of zinc acetate dihydrate to sodium hydroxide (1:1–1:4) was studied.

X-ray diffraction results show the formation of a hexagonal wurtzite zinc oxide structure with a high degree of crystallinity. By increasing the concentration ratio of the reactant raw materials from 1:1 to 1:4, the intensity of the reflection peaks increased and the average size of the as-prepared nanoparticles increased from 20 to 36 nm.

Scanning electron microscopy images show spherical particles, cauliflower-like particles, and irregular cluster morphologies. It can therefore be concluded that the size and morphologies of as-prepared ZnO powders markedly depends on the concentration ratio.

Transmission electron microscopy revealed the size distribution of the nanoparticles. The actual average size of nanoparticles obtained by TEM for a concentration ratio of 1:1 was 18 nm. The ZnO nanoparticles were approximately spherical, confirming the result obtain by SEM. The nanoparticle sizes estimated given XRD, SEM, and TEM are all in good agreement with each other.

Acknowledgment The authors highly appreciate the support provided by the Karaj Branch of Islamic Azad University.

Appendix

No.	Nano structure	Application	Preparation method	Digital object identifier DOI:
1	Nano-arrow	Creating optical or other nanodevices	Atmospheric pressure thermal evaporation	http://dx.doi.org/10.1021/jp050950c
2	Nano-ball	Ultraviolet (UV) lasers	Vapor phase transport	10.3938/jkps.59.129
3	Nano-bottles	Creating optical or other nanodevices	Atmospheric pressure thermal evaporation	10.1021/jp050950c
4	Nano-bowling	Creating optical or other nanodevices	Atmospheric pressure thermal evaporation	10.1021/jp050950c
5	Nano-belts (Quasi-1D)	Piezoelectric	Chemical vapor phase growth	10.1146/annurev.physchem.55.091602.094416
6	Nano-bridges	Optoelectronics	Thermal evaporation and condensation	10.1021/nl025884u
7	Nano-cages (1D)	Efficient sensors	Thermolyzing Zn powders	10.1016/j.actamat.2008.11.022
8	Nano-cable (1D)	Functional building blocks in nanoelectronics/optoelectronics	Thermal reduction	10.1039/B400646A
9	Nano-candle	Building nanodetectors	Atmosphere pressure physical vapor deposition	10.1016/j.jcrysgro.2006.06.049
10	Nano-cone	Sensors	Atmospheric pressure thermal evaporation	10.1016/j.apsusc.2007.02.152 (or 10.1021/jp050950c)
11	Nano-comb	Bio-sensor (glucose detection)	Vapor phase transport	10.1063/1.2210078
12	Nano-cube	Fabrication of optical and optoelectronic nanodevices	Facile hydrothermal	10.1016/j.jallcom.2010.05.055
13	Nano-cluster	Surface acoustic wave (SAW) device fabrication	Matrices of diblock copolymers	10.1016/j.sse.2004.05.052
14	Nano-double teethed comb	Ultraviolet laser	Chemical vapour transport	10.1088/0957-4484/17/8/019
15	Nano-disk	Information storage, transducer, light emitter, catalyst and sensor	Vapor-phase transport	10.1063/1.1811380
16	Nano-ellipsoid like (3D)	Catalysts, sensors and lithium ion electrode materials	Autoclave tests and pyrolysis integrated	10.1088/1674-0068/20/06/613-618
17	Nano-fibers	Gas sensor	Electro-spun from solution	10.4218/etrij.09.1209.0004
18	Nano-flower	Cold cathode electron emission devices	Chemical solution deposition	10.1088/0957-4484/19/31/315202
19	Nano-granular	Gas sensor	Layer-by-layer (LBL) self-assembly	10.1109/INEC.2010.5424971
20	Nano-helix(c)es	One dimensional nanoscale sensors, transducers and resonators	Spontaneous polarization-induced of piezoelectric nanobelts	10.1021/nl034463p
21	Nano-laser	UV nanolaser devices	Vapor phase transport growth	10.1063/1.2805073
22	Nano-multipod	Ultrafast lasing	Chemical vapor transport and condensation	10.1088/0953-8984/21/6/064211
23	Nano-marigold	Field emission sources	Vapour phase deposition	10.1088/0957-4484/17/11/003
24	Nano-needle (1D)	Future photoelectric and flat field emission display devices	Electro-chemical deposition	10.1088/0957-4484/16/11/017
25	Nano-nail	Optoelectronics	Thermal evaporation and condensation	10.1021/nl025884u (or 10.1021/jp050950c)
26	Nano-particle	Catalysts for photo-catalytic degradation	Direct precipitation	10.1016/j.cej.2006.03.003
27	Nano-pillars	Resonator	Chemical vapor deposition	10.1063/1.3549140

No.	Nano structure	Application	Preparation method	Digital object identifier DOI:
28	Nano-powder	Fabrication of third-generation solar cells	Sol–gel process	10.1016/j.solmat.2008.07.015
29	Nano-prism	UV Lasing	Electrochemical process	10.1149/1.2917905
30	Nano-pyramid	Field emission sources	Thermal chemical vapor deposition	10.1016/j.apsusc.2007.05.003
31	Nano-ribbon (1D)	Laser diodes	Thermal reduction process	10.1002/adma2003.05.490
32	Nano-ridges	Inverted polymer solar cell	Sol–gel process	10.1016/j.orgel.2009.08.011
33	Nano-ring	Transducers	Physical evaporation of ZnO powder	10.1063/1.1853514
34	Nano-rod (1D) or 46	Luminescence, field-emission, gas sensing and electron transport	Vapor phase	10.1088/0268-1242/20/4/003
35	Nano-shell	Nanocomposite materials	Hydrothermal synthesis	10.1016/j.cplett.2008.09.042
36	Nano-seed	Schottky barrier ultraviolet (UV) photodetectors	Hydrothermal process	10.1186/1556-276X-6-147
37	Nano-spike	Vacuum microelectronic	Vapor–liquid–solid (VLS)	10.3217/978-3-85125-062-6-466
38	Nano-sphere	Gas sensor	Sol–gel technique	10.1016/j.snb.2009.03.014
39	Nano-spring	Nanoscale electromechanical coupled sensors	Physical evaporation of ZnO powder	10.1063/1.1853514
40	Nano-sheet (2D)	Gas sensing	Hydrothermal process	10.1016/j.snb.2011.03.052
41	Nano-spiral	Electromechanical systems	Thermal evaporation	10.1116/1.2889418
42	Nano-tube (1D)	Dye-sensitized solar cells	Chemical etching	10.1016/j.renene.2010.09.019
43	Nano-tip	Nanoscale optoelectronic device	Soft chemical	10.1016/j.jcrysgro.2004.05.009
44	Nano-tetrapod	Gas-sensing	Evaporation	10.1016/j.cplett.2004.11.091
45	Nano-wall (2D)	Photocatalysts and opto-electronics	Vapor–liquid–solid (VLS)	10.1007/s00339-003-2391-2
46	Nano-wire (1D) or 34	Optical (high transmittancy in the visible wavelengths)	Homoepitaxial electro-deposition	10.1063/1.2711419
47	Nano-whisker (1D) or 46	Micro cavity lasing	Hydrothermal oxidation	10.1063/1.1697633

References

Azaroff LV (1968) Elements of X-ray crystallography. McGraw-Hill, USA

Bhat DK (2008) Facile synthesis of ZnO nanorods by microwave irradiation of zinc–hydrazine hydrate complex. Nanoscale Res Lett 3:31

Cullity BD (1978) Elements of X-ray diffraction. Addison Wesley Publishing Company Inc, USA

Dai ZR, Pan ZW, Wang ZL (2003) Novel nanostructures of functional oxides synthesized by thermal evaporation. Adv Funct Mater 13:9

Hohenberger G, Tomandi G, Ebert R, Taube T (1992) Inhomogeneous conductivity in varistor ceramics: methods of investigation. J Am Ceram Soc 74:2067–2072

Hu XL, Zhu YJ, Wang SW (2004) Sonochemical and microwave-assisted synthesis of linked single-crystalline ZnO rods. Mater Chem Phys 88:421–426

Huang MH, Mao S, Feick H, Yan HQ, Wu YY, Kind H, Weber E, Russo R, Yang PD (2001) Room-temperature ultraviolet nanowire nanolasers. Science 292:1897

Kim JH, Choi WC, Kim HY, Kang YY, Park K (2005) Preparation of mono-dispersed mixed metal oxide micro hollow spheres by homogeneous precipitation in a micro precipitator. Powder Technol 153:166–175

Koch MH, Timbrell PY, Lamb RN (1995) The influence of film crystallinity on the coupling efficiency of ZnO modulator waveguide. Semicond Sci Technol 10:1523–1527

Koh YW, Lin M, Tan CK, Fao YL, Loh KP (2004) Self-assembly and selected growth of ZnO nanorods on any surfaces supported by an aluminum precoat. J Phys Chem B108:11419–11425

Lepkova K, Clohessy J, Cunnane VJ (2007) The pH-controlled synthesis of a gold nanoparticle/polymer matrix via electrodeposition at a liquid–liquid interface. J Phys Condens Mater 19: 375106

Lin HM, Tzeng SJ, Hsiau PJ, Tsai WL (1998) Magnetic and structural properties of nanophase Ag_xFe_{1-x} solid solution particles. Nanostruct Mater 10:465–477

Liu B, Zeng HC (2003) Hydrothermal synthesis of ZnO nanorods in the diameter regime of 50 nm. J Am Chem Soc 125:4430–4431

Nakahara K, Takasu H, Fons P, Yamada A, Matsubara K, Hunger R, Niki S (2001) Interactions between gallium and nitrogen dopants in ZnO films grown by radical-source molecular-beam epitaxy. Appl Phys Lett 79:4139–4141

Okuyama K, Lenggoro IW (2003) Preparation of nanoparticles via spray route. Chem Eng Sci 58:537–547

Park SB, Kang YC (1997) Photocatalytic activity of nanometer size ZnO particles prepared by spray pyrolysis. J Aerosol Sci 28:473–474

Rataboul F, Nayral C, Casanove MJ, Maisonnat A, Chaudret B (2002) Synthesis and characterization of monodisperse zinc and zinc oxide nanoparticles from the organometallic precursor $[Zn(C_6H_{11})_2]$. J Organomet Chem 643(644):307–312

Sahu DR, Lin SY, Huang JL (2007) Deposition of Ag-based Al-doped ZnO multilayer coatings for the transparent conductive electrodes by electron beam evaporation. Sol EnergyMater Sol Cells 91:851–855

Sato T, Tanigaki T, Suzuki H, Saito Y, Kido O, Kimara Y, Kaito C (2003) Structure and optical spectrum of ZnO nanoparticles produced in RF plasma. J Cryst Growth 255:313–316

Singhal M, Chhabra V, Kang P, Shah DO (1997) Synthesis of ZnO nanoparticles for varistor application using Zn-substituted aerosol ot microemulsion. Mater Res Bull 32:239–247

Tokumoto MS, Pulcinelli SH, Santilli CV, Briois V (2003) Catalysis and temperature dependence on the formation of ZnO nanoparticles and of zinc acetate derivatives prepared by the sol-gel route. J Phys Chem B 107:568–574

Tsuzuki T, McCormick PG (2001) ZnO nanoparticles synthesized by mechanochemical processing. Scripta Mater 44:1731–1735

Viswanthan R, Lilly GD, Galer WF, Gupta RB (2003) Formation of zinc oxide–titanium dioxide composite nanoparticles in supercritical water. Ind Eng Chem Res 42:5535–5540

Wang JM, Gao L (2003) Synthesis and characterization of ZnO nanoparticles assembled in one-dimensional order. Inorg Chem Commun 6:877–881

Wang ZL, Song JH (2006) Piezoelectric nanogenerators based on zinc oxide nanowire arrays. Science 14:242–246

Wang ZS, Huang CH, Huang YY, Hou YJ, Xie PH, Zhang BW, Cheng HM (2001) A highly efficient solar cell made from a dye-modified ZnO-covered TiO_2 nanoporous electrode. Chem Mater 13:678–682

West AR (1985) Solid state chemistry and its application. Wiley, New York, pp 174–175

Wu JJ, Liu SC (2002) Low-temperature growth of well-aligned ZnO nanorods by chemical vapor deposition. Adv Mater 14:215–218

Xu JQ, Pan QY, Shun YA, Tian ZZ (2000) Grain size control and gas sensing properties of ZnO gas sensor. Sens Actuators B Chem 66:277–279

Zhang H, Yang D, Ji Y, Ma XY, Xu J, Que DL (2004) Low temperature synthesis of flowerlike ZnO nanostructures by cetyltrimethylammonium bromide-assisted hydrothermal process. J Phys Chem B 18(13):3955–3958

Zhang Z, Yu H, Shao X, Han M (2005) Near-room-temperature production of diameter-tunable ZnO nanorod arrays through natural oxidation of zinc metal. Chem Eur J 11:3149–3154